Design and Evaluation of Coils for a 50 mm Diameter Induction Coilgun Launcher

Ronald J. Kaye, Isaac R. Shokair, and Richard W. Wavrik
Sandia National Laboratories
Albuquerque, NM 87185-1182

James F. Dempsey, William E. Honey, Kenneth J. Shimp
EG&G, Albuquerque, NM 87119

Gary M. Douglas
Rockwell Power Systems, Albuquerque, NM 87102

Abstract — **Coilguns have the ability to provide magnetic pressure to projectiles which results in near constant acceleration. We have developed coils to produce an effective projectile base pressure of 100 MPa (1kbar) as a step toward reaching base pressures of 200 MPa. The design uses a scalable technology applicable to the entire range of breech to muzzle coils of a multi-stage launcher. This paper presents the design of capacitor-driven coils for launching nominal 50 mm, 350 gram projectiles. Design criteria, constraints, mechanical stress analysis, launcher performance, and test results are discussed.**

I. Background

Research at Sandia National Laboratories/New Mexico for the last few years has demonstrated induction coilgun technology in small scale for military and space applications. The coilgun technology may lead to long-range artillery guns or very long launchers that are capable of deploying small satellites into low Earth orbit [1-2]. We are now also developing this technology for applications in transportation and industrial processing.

Our induction coilgun is an electromagnetic launcher which consists of individual magnetic field coils stacked end-to-end to form a barrel. The coils are energized sequentially to generate a travelling wave of magnetic energy that pushes an electrically conducting projectile. The principle of concept, launcher hardware, and description of operation are thoroughly described in a previous paper which also discusses our first litz wire coils [3].

To readily compare the performance of our technology to other guns, we calculate an average effective base pressure, $\bar{P}$, on the projectile. This pressure is the muzzle kinetic energy divided by the barrel volume, or the pressure on the base of the projectile averaged over the barrel length. The instantaneous value of effective base pressure in our gun is

$$\bar{p}(z,t) = \frac{M_p a_p(z,t)}{A_{base}}. \quad (1)$$

where M_p, a_p, and A_{base} are the projectile mass, acceleration, and base area respectively.

Initial tests of encapsulated litz wire cable coils appeared promising. Single layer coils operated successfully at a $\bar{P}$ of 40 MPa (0.4 kbar), but failed to reach the 75 MPa criteria for our next launcher. Applications of interest require pressure near 200 MPa to keep the launcher lengths practical. Mechanical stress analysis, diagnostics of coil deformation, and launcher testing confirmed the need for development of a higher strength coil.

II. Coil Design Goals and Criteria

In August 1992 we elected to develop a new coil in 50 mm scale which would be capable of operating at the magnetic field and stress (mechanical, thermal, and electric) levels required for an average effective base pressure of 200 MPa accelerating 200 mm outer diameter (OD), 60 kg projectiles to 3.5 km/s. The small-scale coil would be designed for low duty-cycle operation to develop an average effective base pressure of 100 MPa over the length of a few coils to demonstrate the technology. A repetitively pulsed design with heat removal will be developed later.

There were several requirements placed on the small-scale coil design. The technology must be scalable at equivalent stress levels, feasible to mechanically model, and use characterized materials and construction techniques. The coil must fit our existing hardware to validate the design with static and moving projectiles.

Desired design features included distributing the simultaneous mechanical, electrical, and thermal stresses, minimizing elastic deformations, and achieving sufficient electric-to-kinetic energy conversion for the launcher to be practical. Ideally the design would allow variation of the number of turns in a coil for applicability to any stage of a launcher.

Manuscript received April 19,1994.
R. J. Kaye, phone 505-845-7658, fax 505-845-7003.
This work was supported by the U.S. Department of Energy under Contract DE-AC04-94AL85000.

0018-9464/95$04.00 © 1995 IEEE

The nature of our coilgun also placed significant constraints on the design. Coils must be closely spaced which limits the size of support structure and generates substantial loads from adjacent, magnetically coupled coils. Coils are therefore an integral part of the support structure.

III. Conceptual Full Scale Design

After reviewing published literature, we analyzed several concepts with analytical techniques and our circuit system model, SLINGSHOT, which is a circuit-based launcher code similar to its predecessor, WARP-10 [4]. The multi-turn machined helix described in Foner is a very robust coil [5]. While such a coil can be self supporting of radial load, straight forward in construction, and provide easy access for heat removal, current concentrations on the inner diameter (ID) of the winding lead to high, localized heating and mechanical stress.

The alternative of nested helices as proposed by Date reduces conductor temperatures and stress concentrations if the conductors are thinner than a current skin depth [6]. At the frequencies of interest for our launcher applications, skin depths are only a few millimeters even in steel conductors. Analysis of launcher performance, which included accounting for current density distributions in the coil windings showed better performance and lower stresses than in a single-layer helix, but the problem of insulating the conductors at high stress and high temperatures remained. Typical average values from these analyses are shown in Table I, where the coil stresses are average loads the winding places on its support structure.

To reduce the temperature and axial pressures, the conductor crossection must be increased and fully utilized by the current. This is possible if the single, skin-depth-size conductor is replaced with a woven litz cable. Results of the conceptual analysis for a multi-layer, litz-cable coil winding showed significant reductions in pressure and temperature. This caused us to develop a method to utilize litz cable construction for our coil design, and overcome its mechanical weaknesses.

Based on our experience utilizing litz cable, failures occur due to wire-to-wire arcing within the cable. An encapsulated litz cable, which is mechanically soft, experiences sufficient strain that the insulation of the individual wires rub against one another. With rectangular compacted litz cable, the wires are crossed to one another generating stress concentrations from loading transverse to the cable axis. If cables are wound adjacent to one another, the overall displacement and strain of the winding can be significant and lead to insulation failure.

To avoid these failure modes, our concept reinforces the litz cable as shown in Fig.1, which is a section view of the small scale coil described below. Round litz cable is used with a low pitch twist to avoid the sharp bend angles and wires crossing each other. To strengthen and stiffen the coil winding, high-strength filaments are built into the litz cable.

TABLE I
Comparison of Conceptual Full Scale Coil Designs

Design Parameter	single helix	nested helices	layered litz cable
B_{pk} (Tesla)	30-35	31	30
$\bar{P}$ (MPa)	150	170	160
Coil σ_r (MPa)	400	420	540
Coil σ_z (MPa)	1300	870	130
ΔT/pulse (°C)	> 600	300	55

Each wire is film insulated then covered with a filament braid to provide wire-to-wire abrasion resistance. The voids of the cable are filled with tows of the filament as the cable is wound and another braid holds the assembly together. Ideally the cable would have the properties of a filament-wound composite when encapsulated.

The litz cable is wound into a multi-layer coil with filament-wound containment shells between the layers. The shells with helical threads provide axial as well as radial support for the round cable. This minimizes the overall deformation of the winding and maintains the shape of the individual cables. There are several documented concepts using shells for reinforcement, but few efforts to integrate

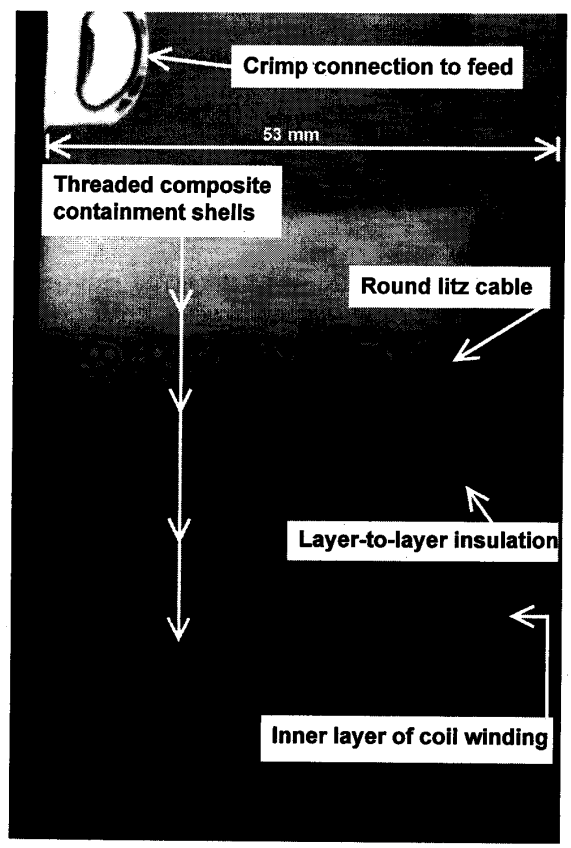

Fig. 1. Section of small scale high field coil.

filament reinforcement into the winding [7-9].

Analysis indicated that all coils of a 800 stage launcher could be designed using this technique, by varying numbers of cables, turns, and wire sizes. Calculations for each of the coils (210 mm ID, 83 mm build, 60 mm long, 75 mm spacing center-to-center, 20% fill fraction) energized with a 43 kV, 1.4 MJ capacitor bank to launch a 60 kg, 200 mm OD projectile, yield the parameters listed for layered litz cable in Table I. Static stress analysis of selected coils indicated that the strains and deformations of the structure were sufficiently low (< 2%), and that this concept could be used for the small scale prototype.

IV. Design of Small Scale Coil

We planned to test five high field coils at the muzzle of our existing 30-stage coilgun capable of accelerating 350 gram, 47 mm OD projectiles to 500 m/s. Ideally the coil dimensions would be scaled from the 200 mm design, but there are requirements and constraints on litz cable construction and mechanical stress in the containment shells which prevent exact scaling.

An analysis coupling scaling relations from previous Slingshot and stress calculations with wire size, cable construction, coil build, and winding geometry optimized cable parameters for projectile performance and coil heating. The tradeoff in the design is conductor fill fraction for strength and stiffness. The high field coil cable is a 6-on-1 spiral winding of 1 mm diameter (18 AWG) copper (UNS C11000) wires with a triple coat of Phelps Dodge Armored Poly-Thermaleze 2000 and a 0.13 mm thick braid of Dupont Kevlar-49. Tows of Kevlar are wound with the braid-covered wire at a 90 mm pitch and held together by an additional Kevlar braid forming the 5 mm OD cable.

The high field coil consists of two litz cables wound in parallel, but 180° apart from one another, forming an 11.5 turn winding in three layers. A section of the coil and the assembly are shown in Figs. 1 and 2. The winding is 57 mm ID, 114 mm OD, and 40 mm long, in a 51 mm ID, 188 mm OD, and 53 mm long structure.

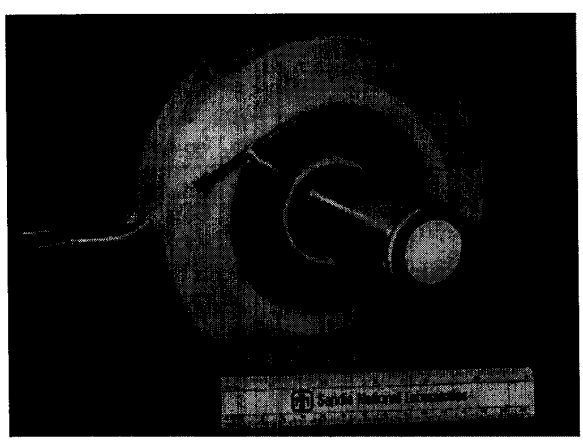

Fig. 2. High field coil assembly with 350 gram, 47 mm OD projectile. Flyway tube to guide projectile not shown.

Each winding layer is supported by a containment shell made of ceramic filament (3M Nextel 440), wet wound with Epon 828/Texaco T-403 resin. Tophat shaped cylinders of heat-shrinkable polyvinyl chloride and polyolefin on the inside of the second and third winding layers insulate for layer-to-layer electrical breakdown. A G10-grade fiberglass laminate plate provides access for the cables to the inner layer of the winding. Upon completion of dry winding and assembly, the coil is vacuum impregnated with a partially-flexiblized, anhydride epoxy.

The coil performance and mechanical response are evaluated separately, but self-consistently. Given coil and projectile geometry and capacitor bank circuit specifications, SLINGSHOT calculates forces on the coil and projectile. The equivalent circuit parameters used for the analysis of the 5 high field coils are given in Fig. 3. Coils are crowbarred at time of peak current to minimize voltage reversal on the capacitors and, with the substantial crowbar resistor, limit coil heating after projectile acceleration. Another version of the SLINGSHOT code, called SLINGSUB, divides coils into series or parallel elements to get localized loads within the coil assembly. Post-processing of the current time histories of coil and projectile elements generates detailed J×B body forces on coil winding elements for stress analysis.

With the EMRC/NISA family of finite-element programs from Engineering Mechanics Research Corporation, we analyzed static stresses to scope cable and shell materials, geometry, and temperature. Many variations were quickly screened using self-consistent loads in single coil models prior to performing dynamic analyses on multi-coil models with the code PRONTO2D, developed at Sandia [10].

To quantify effects of coil and launcher motion, PRONTO2D analyzed transient loaded models of the 5 high field coils. The coil models incorporated body force and static loads, isotropic and orthotropic elastic material properties, and friction at contact surfaces. Figure 4 shows the distribution of axial strain calculated at the time of peak current in stage 34. The projectile is partially through stage 35 which is not yet energized. This type of analysis provided

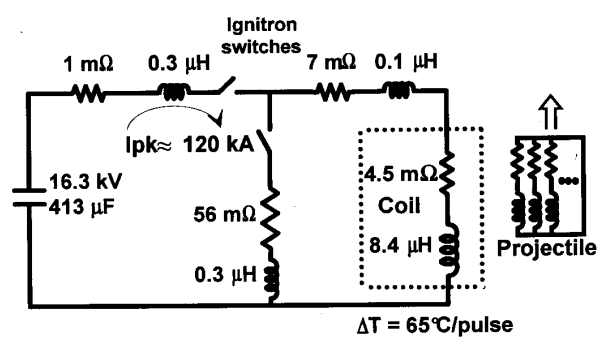

Fig. 3 Capacitor bank and high field coil circuit parameters.

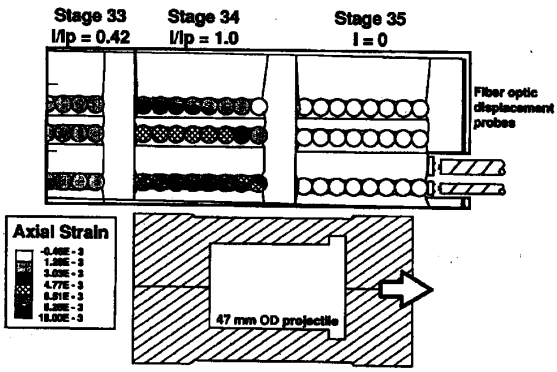

Fig. 4 Axial strain distribution at time of peak current in coil of stage 34. Projectile is entering stage 35 which has not fired yet.

insight to the effects of coil motion from recoil. Table II lists stresses and strains in the inner layer of litz cable winding and the containment shell supporting that layer. These regions of the coil have the greatest loads. The listed values are the maximum from any of the 5 coils accelerating a 350 gram projectile with 100 MPa base pressure in a normal operating mode of the launcher. These stress levels are about 80% of the design point.

V. Coil Evaluation

A single coil testbed was constructed to evaluate the coil design with mechanical, electrical, and thermal diagnostics. Axial and radial reaction loads 20-30% above the normal launch operating condition are developed in the winding with the rear edge of a projectile fixed at the mid plane of the coil. Two types of motion diagnostics were fielded to measure displacement of the coil structure for comparison to the mechanical modeling: a Philtec Fiber Optic Displacement Sensor for internal coil motion, and a Zimmer Optical Displacement Transducer for the external structure.

The Philtec fiber optic displacement sensors utilize bundled glass fibers to transmit to and receive infrared light from reflective targets. A DC-20 kHz bandwidth amplifier produces an analog voltage signal proportional to the distance from the probe to the target over a 2 mm range. We used heat reflecting mirrors as targets to measure axial displacement of the inner layer of the coil winding and its containment shell similar to that shown on the coil in stage 35 in Fig 4. The Zimmer transducer, which tracks the motion of a black-to-white edge, monitored the coil support structure, the Philtec probe holder, and confirmed the Philtec measurements.

The single coil in the test bed was energized with the same circuit shown in Fig. 3, but used 515 μF capacitors and slightly different ignitron switches and cable lengths. Rogowski probes indicated a good current balance to each litz cable of the coil winding. Electrically floating

TABLE II
Maximum Stresses and Strains for Normal Operating Mode

	Inner winding layer	Containment shell
σ_r (MPa)	-193	-166
σ_z (MPa)	-159	-269
σ_φ (MPa)	290	703
total strain (%)	-4.1	-1.3
ΔR/R at ID (%)	1.0	0.6
Δlength/length (%)	-3.8	-1.4

thermocouple probes measured the peak temperature rise near the winding at 0.20 °C/kJ of stored energy and within the composite shells at 0.15 °C/kJ. Tests were repeated as soon as the coil returned to near room temperature through conduction to the structure with about a 30 minute time constant.

After 15 tests with 40 to 80 kJ of stored energy, the working coil was autopsied to examine conditions of the internal structure. There was no deformation of the winding or the containment shells. Although the bond between the inner winding layer and the inside containment shell separated, there was no permanent gap. The inside threads of the containment shells which provide axial support to the winding were intact and not deformed.

Displacement measurements of the muzzle end of the inner winding layer and containment shell #2 showed reasonable agreement with the predicted displacement from PRONTO2D shown in Fig. 5. The general shape of the measured displacement curve from 0 to 300 μs agrees with the calculated curve, but the magnitude of the peak is roughly 2 to 2.5 times lower.

There remains some work that could improve the models and measurements. A small correction may result from using as-built material properties instead of the typical properties from measurements of previous coils. A more important

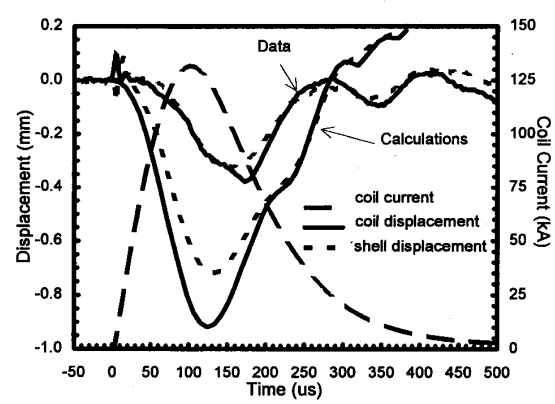

Fig. 5 Displacement calculations and data for muzzle end of inner layer winding and second containment shell. Negative displacement is toward breech end of coil. Stress levels are 20% above normal operating mode launch conditions.

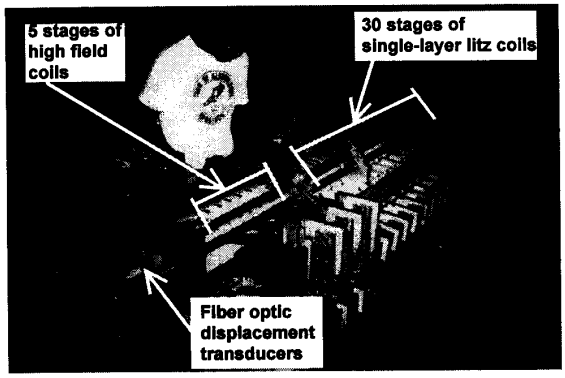

Fig. 6. View of muzzle end of 35-stage launcher.

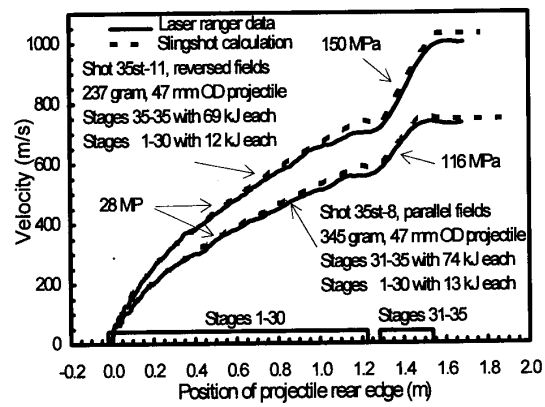

Fig. 7. Comparison of SLINGSHOT code calculations with data.

effect may be visco-elastic stiffening of these materials when loads are suddenly applied. There is a possibility that some of the epoxy used to bond the target mirrors to the coil winding filled the small clearance between the mirror and the G10 plate which may also contribute to a reduction of the measured values.

Figure 6 shows the layout of five high field coils at the muzzle of thirty single-layer litz coils in the launcher support structure. Energy stored in capacitors is delivered through cables on both sides of the gun. Mechanical and electrical diagnostics are similar to those described above. The last coil, stage 35, is instrumented with fiber optic displacement gauges but not thermal diagnostics.

Each coil is energized with a circuit similar to that shown in Fig. 3. The first 30 stages of the launcher have 10.6 μH coils, 171 μF capacitors storing 12 kJ, and crowbar resistances of only a few milliOhms. The circuits for the five high field coils have 513 μF capacitors and slightly greater cabling losses. To reach the field level in the coils required for comparison to the stress analysis, the banks were charged to nominal 70 kJ.

Figure 7 illustrates performance of the launcher and high field coils for differing launch conditions. Projectile velocity is plotted versus position of its rear edge. The 7075-T73 aluminum projectiles are cooled to -196 °C in a liquid nitrogen bath, then loaded into the gun at 10 m/s. The velocity data is derived from a laser ranger which tracks the projectile, and from interrupted pairs of optical beams located before and after the high field coils [3]. Error bands for the velocity measurements are ±5 percent or less. The projectile position data is differentiated once and time averaged with a moving window of 150 μs. Effective base pressure is calculated with (1) using acceleration from the slope of the projectile velocity time history.

In shot 35st-8 shown in Fig. 7, the magnetic field of the five high field coils is oriented parallel to the field direction of the first thirty stages. This is the "normal mode" of operation which minimizes projectile heating. The last five coils developed an average effective base pressure just over 100 MPa even though the capacitor bank on the last stage delivered only 25% of its energy to the coil due to an early crowbar switching. In shot 35st-11, the field of the five high field coils is oriented anti-parallel to the first thirty stages. This "reversed field" mode of operation generates greater projectile acceleration and axial loading on the coil winding with radial loading similar to "normal" operation, but there is significant projectile heating resulting in ablation. The lower mass projectile achieved a velocity of 1.0 km/s while developing an average effective base pressure of 150 MPa.

Overall, there is very good agreement between the SLINGSHOT code simulations and the experiment with only a few areas where deviations exceed 5%. These differences may possibly be random variation of model parameters such as switch resistance, jitter and projectile tracking error. Another source may be second-order effects such as projectile resistance due to thermally and mechanically induced strain of the conductor.

One high field coil failed internally during testing in the "reversed field" mode. A litz cable arced in the region where it transitions from the inner to the middle layer of the winding in one quarter of a turn. The radial support at this point is less than for the bulk of the winding because the azimuthal wound filaments of the containment shell are cut to provide a groove for the cable. Modifications to the filament winding geometry should reinforce this area if the problem is experienced in additional testing. The autopsy of the coil shows the bulk of the winding in very good condition with only a few design changes planned.

VI. Summary

Coilguns must be capable of developing effective base pressure on projectiles comparable to other gun technologies for the potential advantages such as constant acceleration to be useful. We have demonstrated a coil based on reinforcing litz wire cable with high-strength filaments which is capable of averaging 100 MPa base pressure while accelerating 47 mm diameter projectiles to 1 km/s. Calculations show that if

the design is scaled up at the same magnetic field and mechanical stress levels, a coilgun will more efficiently launch 200 mm projectiles with 200 MPa average effective base pressure.

ACKNOWLEDGMENT

The authors thank Finis Long for the development of coil drawings and Robert Davis and Robin Sharpe for their contributions to the coil fabrication process, efforts in fabrication, and launcher maintenance. Thanks to Eugene Cnare for design review, capacitor bank design, and test data analysis; Dean Baca and Roque Feliciano for bank assembly, firing system operation, and diagnostics; Ed Ratliff for bank operation and instrumentation, and Barry Marder, Steve Attaway, and Gerry Wellman for code development. The efforts of Dean Rovang (concept development and review), Dave Van Ornum, Howard Arris, Mike Morrow, Manny Trujillo, (coil fabrication), and Tom Roy at New England Electric Wire and Cable are greatly appreciated.

REFERENCES

[1] R. J. Lipinski, "An electromagnetic induction launcher for Navy applications," Presentation at the Hypervelocity Weapons for Naval Applications and Critical Review of Induction Launcher Technology Meeting, Albuquerque, NM, March 26-27, 1991.

[2] R. J. Lipinski, et. al., "Space applications for contactless coilguns," *IEEE Trans. on Magnetics*, vol. 29, no.1, pp. 691-695, January 1993.

[3] R.J. Kaye, et. al., "Design and Performance of Sandia's Contactless Coilgun for 50 mm Projectiles," *IEEE Trans. on Magnetics*, vol. 29, no. 1, pp. 680-685, January, 1993.

[4] M. M. Widner, "Warp-10: a numerical simulation model for the cylindrical reconnection launcher," *IEEE Trans. on Magnetics*, vol. 27, no.1, pp. 634-638, January, 1991.

[5] S. Foner and H.H. Kolm, "Coil for pulsed Megagauss fields," *Rev. Sci. Instruments*, vol. 27, pp. 547-548, 1956.

[6] A. Yamagishi and M. Date, "High magnetic field facility at Osaka University," *Physica B*, vol. 155, pp. 91-95, 1989.

[7] E.S. Borovik, A.G. Limar, and Yu. A. Litvinenko, "Intense pulsed magnetic fields in reinforced multiturn coils." *Soviet Physics-Technical Physics*, vol. 14, no. 4, pp. 510-511, October, 1969.

[8] L.Van Bockstal, et. al., "Design , fabrication, and testing of internally reinforced coils," Presentation at the 6th Inter. Conf. on Megagauss Magnetic Field Generation and Related Topics, Albuquerque, NM, November 8-11, 1992.

[9] P. P. Mongeau, "Inductively commutated coilguns," *IEEE Trans. on Magnetics*, vol. 27, no.1, pp. 568-572, January 1991.

[10] L. M. Taylor and D. P. Flanagan, "PRONTO2D, a two-dimensional transient solid dynamics program," Sandia Report SAND86-0594, Unlimited release, May, 1992.